Compact wearable dual-mode imaging system for real-time fluorescence image-guided surgery

Nan Zhu
Chih-Yu Huang
Suman Mondal
Shengkui Gao
Chongyuan Huang
Viktor Gruev
Samuel Achilefu
Rongguang Liang

Compact wearable dual-mode imaging system for real-time fluorescence image-guided surgery

Nan Zhu,[a] **Chih-Yu Huang,**[a] **Suman Mondal,**[b] **Shengkui Gao,**[c] **Chongyuan Huang,**[a] **Viktor Gruev,**[c] **Samuel Achilefu,**[b] **and Rongguang Liang**[a,*]
[a]University of Arizona, College of Optical Science, 1630 E. University Boulevard, Tucson, Arizona 85721, United States
[b]Washington University, Department of Radiology, One Bookings Drive, St. Louis, Missouri 63110, United States
[c]Washington University, Department of Computer Science and Engineering, One Bookings Drive, St. Louis, Missouri 63110, United States

Abstract. A wearable all-plastic imaging system for real-time fluorescence image-guided surgery is presented. The compact size of the system is especially suitable for applications in the operating room. The system consists of a dual-mode imaging system, see-through goggle, autofocusing, and auto-contrast tuning modules. The paper will discuss the system design and demonstrate the system performance. © *2015 Society of Photo-Optical Instrumentation Engineers (SPIE)* [DOI: 10.1117/1.JBO.20.9.096010]

1 Introduction

Fluorescence imaging is one of the most popular imaging modalities in biomedical imaging and image-guided surgical systems because of its advantages in high contrast, high sensitivity, low cost, and relatively simple instrumentation.[1–11] Indocyanine green (ICG), as a dye for fluorescence imaging, has been used in retinal angiographs for more than 50 years.[2] In some clinical and surgical applications, ICG imaging is still a relatively new imaging method. ICG can be excited with light around 785 nm and emit fluorescence at longer wavelengths over 800 nm. This near-infrared (NIR) working spectrum is excellent for image-guided surgery because human tissue has less endogenous autofluorescence, less optical absorption, and less scattering.[1–5] However, while ICG fluorescence imaging reveals positions of blood veins and tumors, the resolution is typically low. In addition, ICG fluorescence imaging does not provide detailed information on tissue surfaces. In contrast, white light reflectance imaging provides high-resolution surface information. Thus, white light reflectance imaging and fluorescence imaging are often integrated together because they provide complementary information.[6–11]

Two cameras with different optics are commonly used to capture white light reflectance and NIR fluorescence images separately, but the system is relatively bulky and the fields of view (FOV) are not identical for two imaging modalities.[6] Recently, dual-mode imaging systems with a single sensor have been developed to reduce system complexity.[12,13] Another approach is to capture reflectance image and fluorescence image sequentially with a single camera by modulating the illumination spectrum. The potential issues are the relative image shift between reflectance and fluorescence images and the reduced imaging speed because two images are not captured at the same time and the imaging system is not stationary.

This paper presents a wearable image-guided system for real-time fluorescence image-guided tumor resection and sentinel lymph node mapping. The system consists of a dual-mode imaging system, see-through goggle on a head-mounted display, and mechanisms for autofocusing and auto-contrast adjustment. The autofocusing function is achieved by using microstepper motors and an NIR distance sensor. A pair of liquid crystal glasses are employed to tune the transmission of the see-through channels of the goggle system. The system is capable of working in both visible and NIR modes simultaneously to provide accurate intraoperative visualization of tumors and sentinel lymph nodes in real time. The compact size is especially suitable for applications in the operating room.

2 System Development

The dual-mode imaging system consists of a single all-plastic imaging lens, a dichroic beamsplitter cube, an emission filter, a short-pass filter, a microstepper motor, and two imaging sensors. The camera is able to simultaneously capture both white light and fluorescence images with the same FOV. Two 1/3-inch complementary metal-oxide-semiconductor (CMOS) imaging sensors are used in this dual-mode imaging system: one color sensor (MT9V032C12STC, Aptina Inc, San Jose, California) to capture color images and one monochromatic sensor (MT9V032C12STM, Aptina Inc, San Jose, California) to capture fluorescence images. Both CMOS sensors have 4.51×2.88 mm active image size and 752×480 pixels. Compared to normal charge-coupled device sensors, which have approximately 20% quantum efficiency at 830 nm, the CMOS sensor used in this system has a higher quantum efficiency (>30%) at 830 nm.[14] Each sensor is integrated onto a custom printed circuit board platform. The signals from two sensors are transmitted to a personal computer via a field-programmable gate array integration module with USB communication capabilities (XEM 3050, Opal Kelly, Portland, Oregon).

*Address all correspondence to: Rongguang Liang, E-mail: rliang@optics.arizona.edu

(a)   (b)
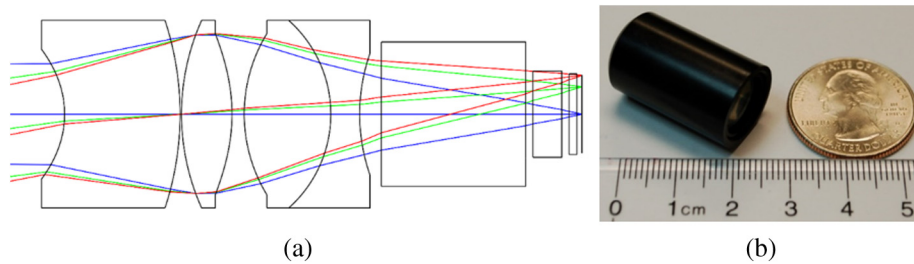
Fig. 1 Custom plastic imaging lens for dual-mode imaging system: (a) lens layout and (b) assembled lens.

(a)   (b)
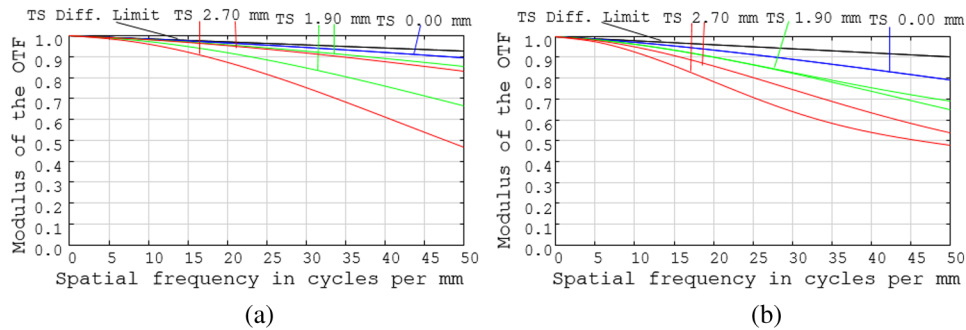
Fig. 2 Modulation transfer functions of the custom plastic imaging lens ($F/\# = 1.75$) in: (a) visible channel and (b) near-infrared (NIR) channel.

2.1 Dual-Mode Camera System with Plastic Lenses

A customized plastic imaging lens was designed and fabricated for this dual-mode imaging system to reduce the weight and size for wearable applications. The lens has a relatively large aperture to simultaneously capture weak fluorescence image and visible image. The detailed lens parameters are as follows: the relative aperture on image space $F/\# = 1.75$, effective focal length = 13.6 mm, full diagonal FOV = 15.5 deg, and working distance = 500 mm. The lens shown in Fig. 1(a) consists of four plastic singlet elements fabricated by a single-point diamond turning machine; the lens diameters are the same to simplify the optomechanical design and lens assembling. The lens surfaces outside the clear apertures for the second and third lenses were purposely fabricated as flat so that it is easier to maintain the distance between the two lenses. Compared to the lens for a single sensor, the challenge of this custom lens is to maintain the long back working distance to accommodate the dichroic beamsplitter, which is used to separate white light

and NIR fluorescence light. As shown in Fig. 1(b), the assembled lens is very compact, thus suitable for wearable applications. For this prototype, the lens tube and the spacers are aluminum; the authors will use black plastic material in the next version to further reduce the weight.

The modulation transfer functions (MTF) of the visible channel and NIR channel of the lens at $F/\# = 1.75$ are shown in Figs. 2(a) and 2(b), respectively. The design MTFs for both visible and NIR channels are sufficiently high for the CMOS sensors to achieve high image quality. The MTF for NIR is slightly better because the bandwidth is narrower than the visible spectrum. Since there is one sensor for each spectrum band, the MTFs in Fig. 2 were optimized with two sensors at different locations. In the experiment, the aperture was reduced to $F/\# = 2.4$ for a longer depth of field.

The configuration and picture of the dual-mode camera are shown in Figs. 3(a) and 3(b). The current size of the camera (with lens) is about $69 \times 24 \times 33$ mm; the length is largely

(a)   (b)
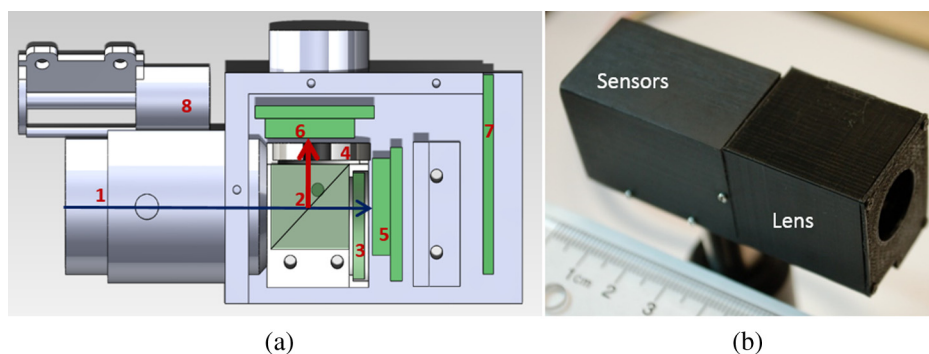
Fig. 3 Compact dual-mode camera. (a) Schematic of internal structure: 1, lens; 2, dichroic beamsplitter; 3, short-pass filter for visible channel; 4, long-pass filter for NIR channel; 5, visible complementary metal-oxide-semiconductor (CMOS) sensor; 6, NIR CMOS sensor; 7, connection board; 8, stepper motor. (b) Assembled dual-mode camera.
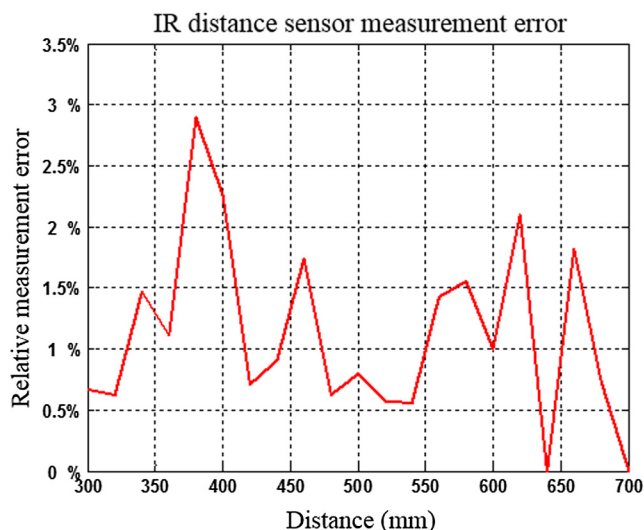
<center>(a)   (b)</center>
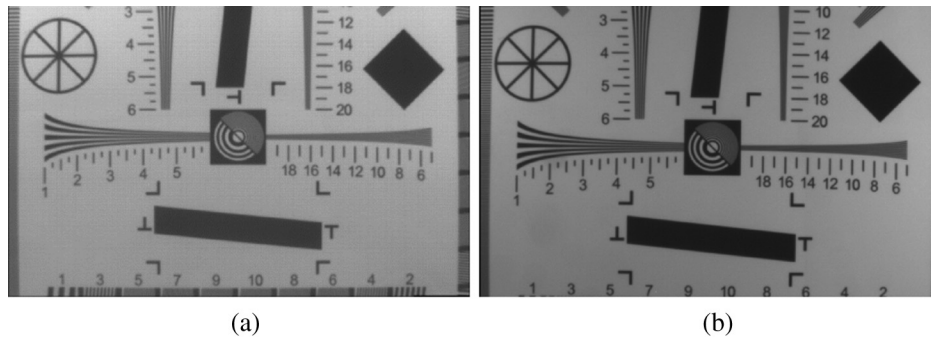
Fig. 4 Resolution chart test of plastic lens F2.4 in: (a) visible channel using two incandescent lamps for illumination and (b) NIR channel using two 850-nm LEDs for illumination.

determined by the electronic board for the sensor. A dichroic beamsplitter cube is used to reflect the NIR fluorescence light to a monochromatic sensor and transmit the visible light to the color camera. A beamsplitter cube, instead of a plate dichroic beamsplitter, is used because the plate beamsplitter will introduce astigmatism, which will degrade image quality. An emission filter is positioned in front of the NIR CMOS sensor to block the excitation light and visible light. Since the visible color CMOS sensor is also sensitive to the NIR light, which will degrade the color performance of the visible image, a short-pass filter is positioned in front of the visible color sensor to block the NIR light with wavelengths longer than 700 nm from the excitation light and surgical light. Figure 4 shows the visible and NIR images of a resolution test chart (1X–I3A/ISO Resolution Test Chart, Edmund Optics, Barrington, New Jersey) positioned 500 mm away from the camera, which is the nominal working distance. The contrast of the visible image is lower than expected due to the stray light introduced by the multiple reflections in the beamsplitter cube and the defocused sensor.

2.2 Autofocus Mechanism

A microstepper motor is used as an actuator to drive the lens forward and backward according to different object distances to achieve autofocusing in real time. An NIR distance sensor

detects the object distance and sends the distance signal to an Arduino single-chip board. A look-up table was established to drive the motor to achieve autofocusing. The autofocusing via stepper motor has the advantage of fast processing compared with the commonly used image-process methods. The average autofocus time for this system is 0.38 s, which is not ideal for image-guided surgery. The authors hope to improve the performance using a high-speed tunable liquid lens in next version.

The accuracy of the NIR distance sensor was measured for object distances from 300 to 700 mm, covering the working range of the imaging system. The relative error of distance measurement is less than 3%, as shown Fig. 5. The relative error is calculated as the ratio of the measurement error and the actual distance. The absolute error is less than 10 mm, comparable to the depth of field of the imaging system.
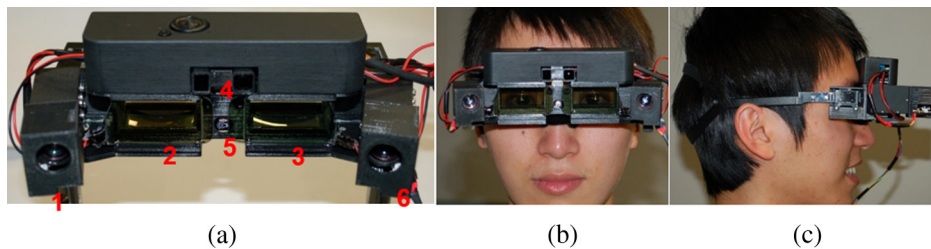
2.3 Goggle System

Figure 6(a) shows the optical layout of the display optics in the goggle; the diagonal field of view is ±23 deg and the pupil size is 6 mm. A Sony OLED Microdisplay with 1280 × 720 pixels is the imager in this head-mounted display. To reduce the weight of the goggle, both the lenses and mirror were designed and fabricated with plastic material (PMMA). The 0.5-mm-thick glass plate beamsplitter is used for its light weight and ability to produce less ghost images. Figure 6(b) shows the resolution test target from microdisplay captured by a SLR camera at the eye pupil position. Figure 7 shows the assembled goggle system with all necessary components. Two cameras are used in this system; it is potentially able to achieve stereo imaging and display. All mechanical components were plastic materials and fabricated using a three-dimensional printer.
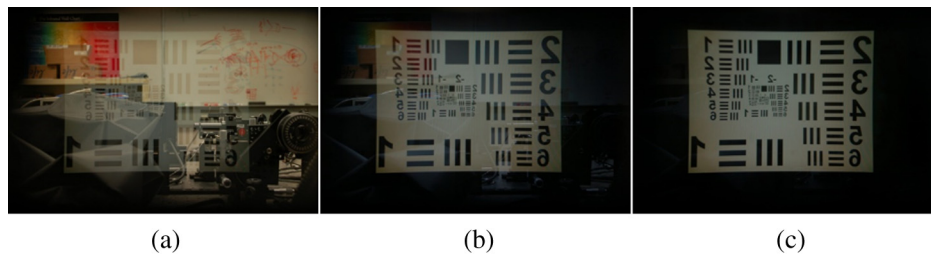
2.4 Tunable Image Contrast

When working in the operating room, the environment in the see-through channel of the goggle is always much brighter than the displayed image in the goggle, resulting in low contrast of displayed fluorescence and visible images. To address this issue, a pair of liquid crystal glasses is positioned in front of the goggle to tune the transmission of the see-through channel. A light sensor is positioned in the middle of the goggle to detect the environment light brightness. The same Arduino single-chip board is used to control the voltage sending to the liquid crystal glass to change the transmission according to the environment brightness. Figures 8(a), 8(b), and 8(c) are images captured with the camera in the eye pupil position when the room light in the lab was on. The resolution target

Fig. 5 The measurement accuracy of the NIR distance sensor.
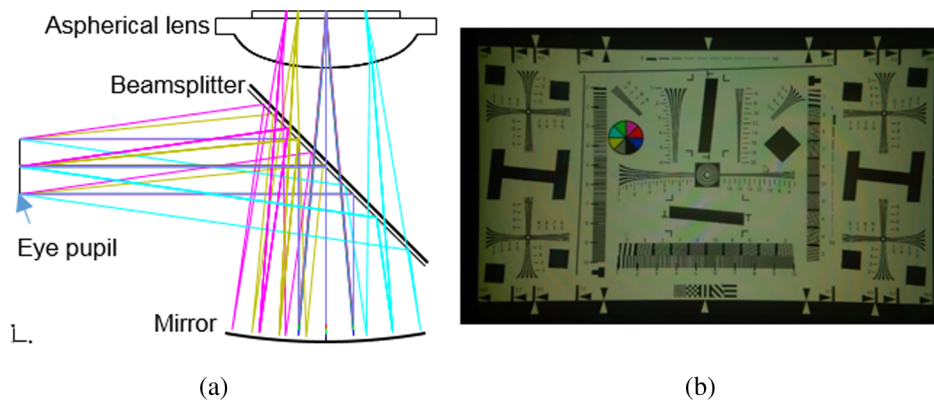
Fig. 6 Display system in the goggle: (a) optical layout and (b) displayed image.

Fig. 7 Assembled goggle system: 1 and 6: dual-mode camera; 2 and 3: liquid crystal; 4: NIR distance sensor; and 5: light sensor.

Fig. 8 Demonstration of the tunable image contrast with different voltage applied to the liquid crystal glass: (a) 0 V, (b) 2.5 V, and (c) 5 V.

was sent to the OLED and displayed by the goggle. Figure 8(a) is the image when no voltage was applied to the liquid crystal, and the liquid crystal had the maximum transmission. While the displayed image from the goggle could be seen, the contrast was very low. When a voltage of 2.5 V was applied on the liquid crystal, the transmitted environment light was reduced significantly, and the contrast of the displayed image from the goggle was much better, as can be seen in Fig. 8(b). When the maximum voltage of 5 V was applied on the liquid crystal, the light from the environment was almost blocked and the best contrast of the displayed image was achieved, as shown in Fig. 8(c).

Figure 9(a) shows the contrast of images from the goggle with different voltages applied to liquid crystal; the region for contrast calculation is shown in Fig. 9(b). As can be seen, when no voltage was applied, the contrast was as low as 0.2, but the contrast increased to 0.75 when maximum voltage was applied to the liquid crystal. This transmission autotunable function is especially useful when the system is working in the operating room because the surgical light is usually very strong.
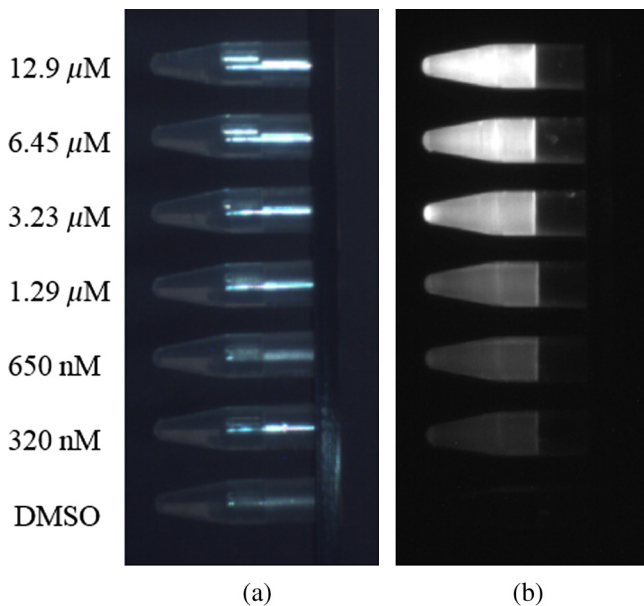
3 System Evaluation

ICG in dimethyl sulfoxide (DMSO) (Sigma-Aldrich, St. Louis, Missouri) was used to test the detection sensitivity of the system. The sensitivity of the proposed system was tested by recording the NIR fluorescence signal responses for different ICG concentrations dissolved in 100% DMSO. The vials with different ICG concentrations were placed 500 mm from the camera. A control vial with pure DMSO was also imaged and denoted as the background signal. The experiment was implemented with ICG concentrations ranging from 130 nM to 5.2 μM.

Both visible and NIR imaging sensors were operating at 27 fps. The NIR image sensor had a maximum exposure time of 30 ms to acquire the best signal-to-noise ratio fluorescence signal. The diluted samples were illuminated with a 785-nm excitation light source, and three different optical powers (2.1, 3.1, and 4.2 mW/cm^2) were used for the system evaluation. Figure 10(a) is the image captured in the visible channel with the excitation light (no visible light was used) and Fig. 10(b) is the NIR fluorescence image. As can be seen from the images,

(a)   (b)
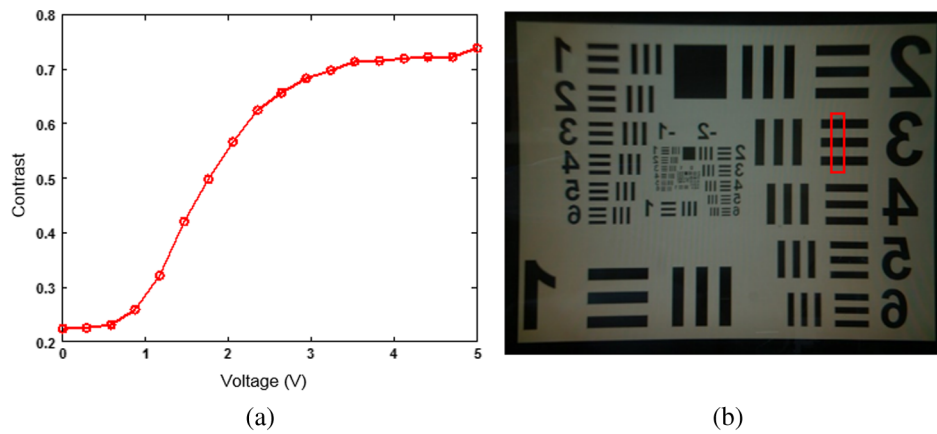
Fig. 9 (a) The contrast of displayed image versus different voltages applied to liquid crystal and (b) the region to calculate the image contrast.

(a)   (b)

Fig. 10 System evaluation with ICG samples: (a) visible image and (b) fluorescence image of ICG samples with different concentrations.
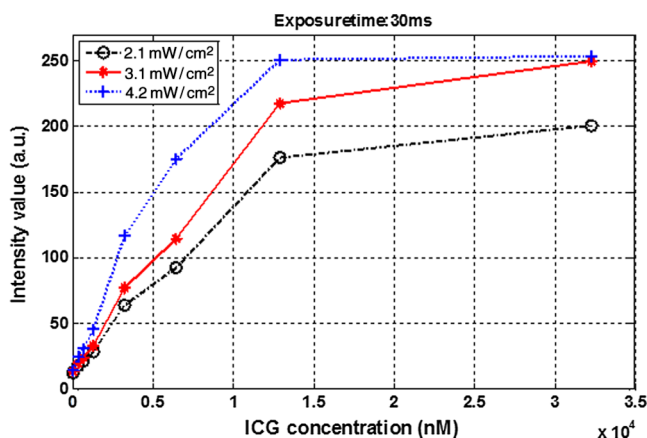
Fig. 11 Sensitivity test using indocyanine green (ICG) samples with different ICG concentrations.

some excitation light leaked into the visible imaging channel. In NIR channel, the vial with pure DMSO is not visible, indicating that the excitation light was blocked by the emission filter. Figure 11 shows the signal intensity in linear scale for different ICG concentrations ranging from 500 pM to 50 μM, showing the system has good sensitivity for surgical applications.

4 Conclusion

This paper presents a wearable dual-mode wearable imaging system for real-time fluorescence image-guided surgery. The compact size of the system is especially suitable for applications in the operating room. The system is capable of working simultaneously in both visible and NIR channels. To address the practical needs, the authors integrated autofocusing and contrast adjustment in the system. The feasibility of the system has been demonstrated with ICG samples. In the future, the authors plan to improve the autofocusing speed with a high-speed tunable liquid lens.

References

1. A. L. Vahrmeijer et al., "Image-guided cancer surgery using near-infrared fluorescence," *Nat. Rev. Clin. Oncol.* **10**(9), 507–518 (2013).
2. M. V. Marshall et al., "Near-infrared fluorescence imaging in humans with indocyanine green: a review and update," *TOSOJ* **2**(2), 12–25 (2010).
3. K. E. Adams et al., "Comparison of visible and near-infrared wavelength-excitable fluorescent dyes for molecular imaging of cancer," *J. Biomed. Opt.* **12**(2), 024017 (2007).
4. E. M. Sevick-Muraca, "Molecular imaging with optics: primer and case for near-infrared fluorescence techniques in personalized medicine," *J. Biomed. Opt.* **13**(4), 041303 (2008).
5. S. Gioux, H. S. Choi, and J. V. Frangioni, "Image-guided surgery using invisible near-infrared light: fundamentals of clinical translation," *Mol. Imaging* **9**(5), 237–55 (2010).
6. X. Wang et al., "Compact instrument for fluorescence image-guided surgery," *J. Biomed. Opt.* **15**(2), 020509 (2010).

7. Y. Liu et al., "Near-infrared fluorescence goggle system with complementary metal-oxide-semiconductor imaging sensor and see-through display," *J. Biomed. Opt.* **18**(10), 101303 (2013).

8. S. Gao et al., "Image overlay solution based on threshold detection for a compact near infrared fluorescence goggle system," *J. Biomed. Opt.* **20**(1), 016018 (2015).

9. S. B. Mondal et al., "Real-time fluorescence image-guided oncologic surgery," *Adv. Cancer Res.* **124**, 171–211 (2014).

10. N. Zhu et al., "Engineering LED surgical light for NIR fluorescence image-guided surgical systems," *J. Biomed. Opt.* **19**(7), 076018 (2014).

11. N. Zhu et al., "Dual-mode optical imaging system for fluorescence image-guided surgery," *Opt. Lett.* **39**(13), 3830–3832 (2014).

12. Z. Chen, X. Wang, and R. Liang, "RGB-NIR multispectral camera," *Opt. Express* **22**(5), 4985–4994 (2014).

13. Z. Chen et al., "Single camera imaging system for color and near-infrared fluorescence image guided surgery," *Biomed. Opt. Express* **5**(8), 2791–2797 (2014).

14. https://www.aptina.com/products/image_sensors/mt9v032d00stm/.

Biographies for the authors are not available.